Available online at www.sciencedirect.com
SCIENCE DIRECT®
C. R. Geoscience 338 (2006) 476–487
COMPTES RENDUS GEOSCIENCE
http://france.elsevier.com/direct/CRAS2A/

Geomaterials (Mineralogy)

Green rusts in electrochemical and microbially influenced corrosion of steel

Philippe Refait [a,*], Mustapha Abdelmoula [b], Jean-Marie R. Génin [b], René Sabot [a]

[a] *Laboratoire d'étude des matériaux en milieux agressifs (LEMMA), EA 3167, université de La Rochelle, bât. Marie-Curie, av. Michel-Crépeau, 17042 La Rochelle cedex 01, France*

[b] *Laboratoire de chimie physique et microbiologie pour l'environnement (LCPME), UMR 7564, CNRS–université Henri-Poincaré–Nancy-1, 405, rue de Vandoeuvre, 54600 Villers-lès-Nancy, France*

Received 7 March 2006; accepted after revision 9 March 2006

Available online 5 June 2006

Written on invitation of the Editorial Board

Abstract

Green rusts have been identified as corrosion products of steel in neutral or slightly alkaline aqueous media. They were mainly observed in carbonated media, where the carbonated green rust is obtained, and in seawater, where the sulphated variety is obtained. In the first case, the formation of the carbonated green rust competes with that of siderite $FeCO_3$. It is favoured when the dissolution of iron is accompanied by the reduction of dissolved oxygen and the formation of OH^- ions. In the second case, the formation of the sulphated variety competes with that of the chlorinated variety. The sulphated green rust is obtained since the layered structure of green rusts is characterised by a strong affinity for divalent anions. Finally, the oxidation of green rusts leads to the various constituents of 'common' rust. The conditions favouring the formation of a ferric compound keeping the crystal structure of green rusts is discussed. ***To cite this article: P. Refait et al., C. R. Geoscience 338 (2006).***

Résumé

Les rouilles vertes en corrosion électrochimique et microbiologique des métaux ferreux. Les rouilles vertes ont été identifiées en tant que produits de corrosion du fer et des aciers dans des milieux aqueux neutres ou légèrement basiques. Il s'agit principalement de milieux carbonatés, où la variété carbonatée des rouilles vertes est donc observée, et du milieu marin, où se forme la variété sulfatée. Dans le premier cas, la formation de la rouille verte carbonatée entre en compétition avec celle de la sidérite $FeCO_3$. Elle est favorisée lorsque la réduction de l'oxygène dissous permet la formation d'ions OH^- simultanément à la dissolution du fer. Dans le second cas, la formation de la rouille verte sulfatée entre en compétition avec celle de son analogue chloruré. La formation de la variété sulfatée découle de l'affinité de la structure lamellaire des rouilles vertes pour les anions divalents. L'oxydation des rouilles vertes conduit enfin aux différents constituants de la « rouille » commune. Les conditions permettant la formation d'un composé ferrique conservant la structure de type rouille verte sont discutées. ***Pour citer cet article : P. Refait et al., C. R. Geoscience 338 (2006).***

* Corresponding author.
E-mail address: philippe.refait@univ-lr.fr (P. Refait).

1631-0713/$ – see front matter © 2006 Académie des sciences. Published by Elsevier SAS. All rights reserved.
doi:10.1016/j.crte.2006.04.012

Keywords: Carbonated media; Seawater; Sulphate; Marine corrosion; Ferric green rusts

Mots-clés : Milieux carbonatés ; Eau de mer ; Sulfate ; Corrosion marine ; Rouilles vertes ferriques

1. Introduction

The $Fe^{II–III}$ hydroxycarbonate, that is the carbonated form of green rusts, $GR(CO_3^{2-})$, was discovered as a corrosion product of steel in an urban water pipe [47]. The role of GRs in the degradation of iron-based materials has been underestimated until recently following the discovery of $GR(CO_3^{2-})$, which indicated that GRs could form in various environments from various materials. For instance, they were observed as corrosion products of mild steels in boiling chloride or sulphate containing solutions [9] or of cast iron in NaCl, K_2SO_4 and Na_2CO_3 solutions at room temperature [24]. They were identified later amongst the products of pitting corrosion processes of stainless steels and related iron alloys [6,7]. And finally, the most severe cases of microbially induced corrosion of carbon steels in seawater, at that time attributed to sulphate reducing bacteria, are somehow associated with the hydroxysulphate $GR(SO_4^{2-})$ [14,31].

The estimation of the standard Gibbs free energy of formation of GRs allowed us to draw potential–pH equilibrium Pourbaix diagrams, where the GR compounds are included [11,13,15,33]. It was the first step towards the full understanding of the importance of GRs in corrosion processes. It predicted that in solutions with moderate concentrations (∼0.01–0.1 M) of Cl^-, SO_4^{2-} or HCO_3^-/CO_3^{2-}, the corresponding GR would form in neutral and slightly alkaline media (pH∼ 7–11). A series of experimental studies confirmed this analysis. The corrosion of iron and steel in adequate media, either at open circuit potential or under electrochemical polarisation, led to GRs as predicted. The simplest experiment, that is the immersion of an iron disk in solution, was achieved in 0.1 M $NaHCO_3$ and 0.1 M $NaHCO_3 + 4$ M NaCl electrolytes. Homogeneous layers of $GR(CO_3^{2-})$ were observed in each case [1]. Potentiostatic polarisation was applied to an iron electrode immersed in a 1 M KCl solution of pH about 9. Depending on the applied potential value, the main corrosion product was $Fe(OH)_2$ or $GR(Cl^-)$, in agreement with the corresponding Pourbaix diagram [38]. Galvanostatic polarisation applied to iron electrodes immersed in various concrete-simulating electrolytes also produced GRs [16]. And finally, $GR(SO_4^{2-})$ was identified in seawater corrosion problems [40,43]. This is due to the fact that even if the seawater Cl^-/SO_4^{2-} molar ratio is about 19, the affinity of the GR crystal structure for divalent anions is stronger, e.g., $GR(SO_4^{2-})$, than for monovalent anions, e.g., $GR(Cl^-)$ [40].

The oxidation of GRs can lead to the most common constituents of rust, that is goethite, lepidocrocite, akaganeite and magnetite, depending on pH, temperature, oxygen flow, dissolved Fe^{II} concentration and, more generally, composition of the electrolyte [10–13,15,28,29,32,38,40]. But Fe^{II} cations can also be completely oxidised in situ, by leaving essentially unchanged the initial layered structure and leading to what was called 'ferric green rust', as obtained by deprotonation of OH^- ions that surround Fe cations [34,41]. This new compound was discovered as the result of the action of hydrogen peroxide upon GRs, but was also obtained by oxidation of a dry GR layer [1] or anodic polarisation of steel [22].

In this article, the mechanisms of formation of GRs from steel are discussed. Two main types of aqueous media are considered, the carbonated media representing freshwaters, and the chloro-sulfated media representing seawater. In the first case, the competition between $GR(CO_3^{2-})$ and $FeCO_3$ siderite is stressed. In the second case, the competition between both types of GRs, $GR(SO_4^{2-})$ and $GR(Cl^-)$, is studied. Finally, the conditions that favour the formation of 'ferric green rusts' are discussed.

2. Methodology

When a steel electrode is corroding in an aerated electrolyte, the potential, called open-circuit potential (OCP), reaches a value somewhere between the potential of Fe^{II}/Fe equilibrium and that of O_2/H_2O equilibrium. The corrosion process can be accelerated electrochemically by increasing either the potential of the electrode, i.e. the potentiostatic procedure, or the current flowing through the electrode, i.e. the galvanostatic procedure. Such experiments can be devised in the laboratory for monitoring the early stages of the corrosion process. In this article, experiments performed at OCP using E24 steel (98.2% Fe, 0.122% C, 0.206% Si, 0.641% Mn, 0.016% P, 0.131% S, 0.118% Cr, 0.02% Mo, 0.105% Ni and 0.451% Cu) are described. The steel surfaces were polished with silicon carbide (particle size 25 μm), rinsed thoroughly with Milli-Q water and carefully dried. The potential was measured using an Ametek (Princeton Applied Research) 263/A potentiostat system. A saturated calomel electrode (SCE) was used as a reference, but the potential is expressed with respect to the standard hydrogen electrode (SHE) in order to facilitate the comparison with potential–pH equilibrium Pourbaix diagrams.

The kinetics of degradation of steel tends to decrease as the metal is covered by a rust layer and the behaviour of a steel structure dipped in water for years is governed by the properties of this several-millimetre-thick layer. The understanding of the mechanisms at such late stages of the corrosion process requires a detailed analysis of the morphology and composition of the rust layers. The case of a steel structure left for 25 years in the Atlantic Ocean is detailed. The identification of transient unstable phases such as GRs is only made possible if the samples are sheltered immediately from oxygen. Therefore, the corrosion layers, about 10–15-mm thick, scrapped from the metal in the permanently immersed zone, 1 m above the mud line, were immediately placed in acetone, preventing any chemical evolution of the samples for 3–4 months. They were coated with epoxy resin (Struers Epofix®), sawed up into 2-mm-thick slices, and again coated with resin. Cuts were achieved so that slices were perpendicular to the steel/rust layer interface. More details concerning this procedure can be found elsewhere [25].

Additional information about the mechanisms of formation and transformation of rust can be obtained via the study of the oxidation of a Fe(II) precipitate in aqueous suspension [10–13,15,33,38,40]. The oxidation processes involved in chloro-sulfated media were then studied using the following methodology. $FeCl_2 \cdot 4\,H_2O$ and $FeSO_4 \cdot 7\,H_2O$ were dissolved in a 100-ml flask of milliQ water. The $\{[Cl^-]/[SO_4{}^{2-}]\}$ ratio was set at $1/12$. NaOH was dissolved in another 100-ml flask and two $\{[Fe^{2+}]/[OH^-]\}$ ratios were considered, 1 and 0.58. The NaOH concentration was set at 0.4 M, and the temperature at 25 °C. The solutions were mixed, leading to the precipitation of a Fe(II) compound. Magnetic stirring (∼500 rpm) in the open air ensured a progressive homogeneous oxidation of the precipitate and a thermostat controlled the temperature, which was kept at 25 ± 0.5 °C. Reactions were monitored by recording the pH, measured via a glass electrode, and the potential E of a platinum electrode immersed in solution, using the saturated calomel electrode as a reference (but all potentials in the following refer to the standard hydrogen electrode, SHE).

3. Rust layer characterisation

Different characterisation methods must be combined to identify unambiguously the various components of a rust layer. X-ray diffraction (XRD) can be used along with Raman and/or Mössbauer spectroscopy. Here, analyses performed by XRD, conversion electron Mössbauer spectroscopy (CEMS) and micro-Raman spectroscopy are presented.

3.1. CEMS

The decay of the nuclear excited state of ^{57}Fe leads to the emission and subsequent resonant absorption of 14.4-keV photons. These are the photons that are not detected in the Mössbauer effect transmission measurements and correspond to the usual negative peaks of the Mössbauer spectra. The principle of CEMS is based upon the detection of the internally converted electrons emitted after the resonant absorption of γ-rays has taken place. This emission of K-conversion electrons with 7.3-keV energy is detected in backscattering experiments and is adequate for a non-destructive surface analysis. The analysed depth is about 300 nm. A room-temperature spectrum presented here was recorded using a gas flow proportional counter. The constant-acceleration Mössbauer spectrometer was calibrated with an α-Fe disk. The spectra were computer-fitted with a sum of Lorentzian shape lines. Errors on the Mössbauer parameters are about ± 0.02 mm s^{-1} for isomer shift δ and quadrupole splitting Δ and ± 2 kOe for hyperfine field H.

3.2. XRD

Products were also analysed by XRD using Co Kα_1 wavelength ($\lambda = 0.17889$ nm) in Bragg–Brentano geometry. Reactive compounds such as GRs are coated with glycerol to avoid any oxidation [18].

3.3. Raman spectroscopy

The Raman study of the marine corrosion products of steel was performed using a multichannel DILOR OMARS 89 spectrometer®. The apparatus is fitted with a diode array detection system, which enables a 500-cm^{-1} broad spectrum to be analysed for a typical acquisition time of 30 s. Excitation of the samples was carried out with 514.5-nm radiation from a Spectra Physics 2017® argon ion laser. The power of the source was 20 mW and the spectral resolution was 3 cm^{-1}.

4. Fresh water and GR($CO_3{}^{2-}$)

E–pH Pourbaix diagrams are maps that summarise the thermodynamic information describing the possible

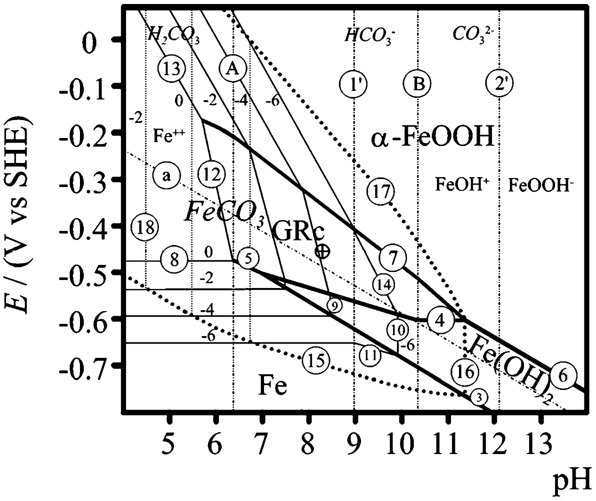

Fig. 1. Superimposition of Pourbaix diagrams of iron in carbonate-containing aqueous solution at 25 °C, for an activity of carbonate species of 0.1. GRc designates $GR(CO_3{}^{2-})$. The diagram in solid line was drawn omitting $FeCO_3$, the diagram in dotted lines was drawn considering each solid phase.

Fig. 1. Superposition des diagrammes de Pourbaix du fer en solution aqueuse carbonatée à 25 °C, pour une activité des espèces carbonate de 0,1. GRc désigne $GR(CO_3{}^{2-})$. Le diagramme en ligne pleine est tracé en omettant $FeCO_3$, le diagramme en pointillé est tracé en considérant chaque phase solide.

routes followed during the corrosion of steels in carbonated aqueous media (Fig. 1). Values of the standard Gibbs energy of formation ΔG_f^0 that are retained for the various species are listed in Table 1 and the equilibrium equations are reported in Table 2. For Fe species, the ΔG_f^0 values were taken from [5,20], or re-computed from solubility products using the value $\Delta G_f^0(Fe^{2+}{}_{aq})$ of Table 1. This allowed us to have a complete set of consistent values and equations. The ΔG_f^0 value of $FeCO_3$ was computed from the solubility product ($-\log K_{so}$) value of −10.80 given by [8], but values ranging from −10.43 to −11.20 are reported [19]. The other values were taken from Wagman et al. [48]. The diagrams were drawn using an activity of carbonate species equal to 0.1. A first diagram was drawn considering $GR(CO_3{}^{2-})$, but ignoring $FeCO_3$. It is represented in solid lines. The second diagram was drawn considering both phases. Equilibrium reactions involving $FeCO_3$ are represented in dotted lines. The domain of stability of $GR(CO_3{}^{2-})$ is totally included inside that of $FeCO_3$, which is delimited by lines (15), (16), (17) and (18). This demonstrates that the hydroxycarbonate $GR(CO_3{}^{2-})$ is metastable with respect to $FeCO_3$.

However, it was reported that homogeneous $GR(CO_3{}^{2-})$ layers could form on iron disks dipped in 0.1 M $NaHCO_3$ solutions [1]. This experiment was performed again, using a 30-mm diameter E24 steel disk. The OCP of the disk was measured during the 24 h of immersion. It decreased from about +50 mV_{SHE} down to about −450 mV_{SHE}, while the initial Fe_2O_3 film formed in air upon the steel surface dissolved.

Table 1
Gibbs free energies of formation used for calculations in standard temperature and pressure conditions

Tableau 1
Enthalpies libres de formation utilisées pour les calculs dans les conditions standard de température et de pression

Species	Average oxidation number of Fe	ΔG_f^0 (kJ mol^{-1})	References
Solid species			
α-Fe	0	0	
$Fe(OH)_{2(s)}$	+2	−492	[5,20]
$FeCO_{3(s)}$	+2	−681	Computed from [8]
$GR(CO_3{}^{2-})$, that is [12]: $Fe^{II}{}_4Fe^{III}{}_2(OH)_{12}CO_3{\cdot}2H_2O_{(s)}$	+7/3	−4076	Computed from [13] using ΔG_f^0 of $Fe(OH)_{2(s)}$ given above
α-$FeOOH_{(s)}$	+3	−485.3	[5]
Liquid and dissolved species			
H_2O	—	−237.18	[5,20]
$Fe^{2+}{}_{aq}$	+2	−91.5	[5,20]
$FeOH^+$	+2	−277.4	[5,20]
$FeOOH^-$	+2	−376.4	[5,20]
H_2CO_3	—	−623.2	[48]
$HCO_3{}^-$	—	−586.8	[48]
$CO_3{}^{2-}$	—	−527.9	[48]

Table 2
Equilibrium equations of E–pH Pourbaix diagrams drawn in Fig. 1
Tableau 2
Équations d'équilibre des diagrammes de Pourbaix E–pH de la Fig. 1

Water and carbonate system

(a) $H_2 \rightleftharpoons 2\,H^+ + 2\,e^-$
$E = 0.000–0.059$ pH
(A) $H_2CO_3 \rightleftharpoons HCO_3{}^- + H^+$
$6.37 = \log[H_2CO_3] - \log[HCO_3{}^-] + pH$
(B) $HCO_3{}^- \rightleftharpoons CO_3{}^{2-} + H^+$
$10.34 = \log[HCO_3{}^-] - \log[CO_3{}^{2-}] + pH$

Fe–H_2O system

(1′) $Fe^{2+} + H_2O \rightleftharpoons FeOH^+ + H^+$
$8.98 = \log[Fe^{2+}] - \log[FeOH^+] + pH$
(2′) $FeOH^+ + H_2O \rightleftharpoons FeOOH^- + 2\,H^+$
$12.10 = 0.5\log[FeOH^+] - 0.5\log[FeOOH^-] + pH$
(3) $Fe + 2\,H_2O \rightleftharpoons Fe(OH)_2 + 2\,H^+ + 2\,e^-$
$E = -0.091–0.0591$ pH
(4) (a) $6\,Fe(OH)_2 + CO_3{}^{2-} + 2\,H_2O \rightleftharpoons Fe_6(OH)_{12}CO_3{\cdot}2\,H_2O + 2\,e^-$
$E = -0.63 - 0.0296\log[CO_3{}^{2-}]$
(b) $6\,Fe(OH)_2 + HCO_3{}^- + 2\,H_2O \rightleftharpoons Fe_6(OH)_{12}CO_3{\cdot}2\,H_2O + H^+ + 2\,e^-$
$E = -0.33 - 0.0296\log[HCO_3{}^-] - 0.0296\,pH$
(5) $6\,Fe + HCO_3{}^- + 14\,H_2O \rightleftharpoons Fe_6(OH)_{12}CO_3{\cdot}2\,H_2O + 13\,H^+ + 14\,e^-$
$E = -0.12 - 0.0042\log[HCO_3{}^-] - 0.0549\,pH$
(6) $Fe(OH)_2 \rightleftharpoons \alpha\text{-}FeOOH + H^+ + e^-$
$E = 0.069–0.0591$ pH
(7) (a) $Fe_6(OH)_{12}CO_3{\cdot}2\,H_2O \rightleftharpoons 6\,\alpha\text{-}FeOOH + 2\,H_2O + CO_3{}^{2-} + 6\,H^+ + 4\,e^-$
$E = 0.42 + 0.0148\log[CO_3{}^{2-}] - 0.0887\,pH$
(b) $Fe_6(OH)_{12}CO_3{\cdot}2\,H_2O \rightleftharpoons 6\,\alpha\text{-}FeOOH + 2\,H_2O + HCO_3{}^- + 5\,H^+ + 4\,e^-$
$E = 0.27 + 0.0148\log[HCO_3{}^-] - 0.0739\,pH$
(c) $Fe_6(OH)_{12}CO_3{\cdot}2\,H_2O \rightleftharpoons 6\,\alpha\text{-}FeOOH + 2\,H_2O + H_2CO_3 + 4\,H^+ + 4\,e^-$
$E = 0.17 + 0.0148\log[H_2CO_3] - 0.0591\,pH$
(8) $Fe \rightleftharpoons Fe^{2+} + 2\,e^-$
$E = -0.474 + 0.0296\log[Fe^{2+}]$
(9) $Fe^{2+} + 2\,H_2O \rightleftharpoons Fe(OH)_2 + 2\,H^+$
$12.94 = \log[Fe^{2+}] + 2\,pH$
(10) $FeOH^+ + H_2O \rightleftharpoons Fe(OH)_2 + H^+$
$3.96 = \log[FeOH^+] + pH$
(11) $Fe + H_2O \rightleftharpoons FeOH^+ + H^+ + 2\,e^-$
$E = -0.21 + 0.0296\log[FeOH^+] - 0.0296\,pH$
(12) (a) $6\,Fe^{2+} + HCO_3{}^- + 14\,H_2O \rightleftharpoons Fe_6(OH)_{12}CO_3{\cdot}2\,H_2O + 13\,H^+ + 2\,e^-$
$E = 1.97 - 0.1773\log[Fe^{2+}] - 0.0296\log[HCO_3{}^-] - 0.3842\,pH$
(b) $6\,Fe^{2+} + H_2CO_3 + 14\,H_2O \rightleftharpoons Fe_6(OH)_{12}CO_3\ {\cdot}2\,H_2O + 14\,H^+ + 2\,e^-$
$E = 2.16 - 0.1773\log[Fe^{2+}] - 0.0296\log[H_2CO_3] - 0.4137\,pH$
(13) $Fe^{2+} + 2\,H_2O \rightleftharpoons \alpha\text{-}FeOOH + 3\,H^+ + e^-$
$E = 0.83 - 0.059\log[Fe^{2+}] - 0.1773\,pH$
(14) $6\,FeOH^+ + HCO_3{}^- + 8\,H_2O \rightleftharpoons Fe_6(OH)_{12}CO_3{\cdot}2\,H_2O + 7\,H^+ + 2\,e^-$
$E = 0.38 - 0.1773\log[FeOH^+] - 0.0296\log[HCO_3{}^-] - 0.2068\,pH$
(15) (a) $Fe + CO_3{}^{2-} \rightleftharpoons FeCO_3 + 2\,e^-$
$E = -0.793 - 0.0296\log[CO_3{}^{2-}]$
(b) $Fe + HCO_3{}^- \rightleftharpoons FeCO_3 + H^+ + 2\,e^-$
$E = -0.488 - 0.0296\log[HCO_3{}^-] - 0.0296\,pH$
(c) $Fe + H_2CO_3 \rightleftharpoons FeCO_3 + 2\,H^+ + 2\,e^-$
$E = -0.300 - 0.0296\log[H_2CO_3] - 0.0591\,pH$
(16) $FeCO_3 + 2\,H_2O \rightleftharpoons Fe(OH)_2 + CO_3{}^{2-} + 2\,H^+$
$23.73 = 2\,pH - \log[CO_3{}^{2-}]$

(*continued on next page*)

Table 2 (*continued*)

(17)	(a)	$FeCO_3 + 2H_2O \rightleftharpoons \alpha\text{-}FeOOH + CO_3{}^{2-} + 3H^+ + e^-$
		$E = 1.473 + 0.0591 \log[CO_3{}^{2-}] - 0.1773\,pH$
	(b)	$FeCO_3 + 2H_2O \rightleftharpoons \alpha\text{-}FeOOH + HCO_3{}^- + 2H^+ + e^-$
		$E = 0.863 + 0.0591 \log[HCO_3{}^-] - 0.1182\,pH$
	(c)	$FeCO_3 + 2H_2O \rightleftharpoons \alpha\text{-}FeOOH + H_2CO_3 + H^+ + e^-$
		$E = 0.486 + 0.0591 \log[H_2CO_3] - 0.0591\,pH$
(18)	(a)	$Fe^{2+} + HCO_3{}^- \rightleftharpoons FeCO_3 + H^+$
		$-0.47 = \log[Fe^{2+}] + \log[HCO_3{}^-] + pH$
	(b)	$Fe^{2+} + H_2CO_3 \rightleftharpoons FeCO_3 + 2H^+$
		$5.90 = \log[Fe^{2+}] + \log[H_2CO_3] + 2\,pH$
(19)	(a)	$6FeCO_3 + 14H_2O \rightleftharpoons Fe_6(OH)_{12}CO_3{\cdot}2H_2O + 5CO_3{}^{2-} + 12H^+ + 2e^-$
		$E = 2.055 + 0.1475 \log[CO_3{}^{2-}] - 0.355\,pH$
	(b)	$6FeCO_3 + 14H_2O \rightleftharpoons Fe_6(OH)_{12}CO_3{\cdot}2H_2O + 5HCO_3{}^- + 7H^+ + 2e^-$
		$E = 3.58 + 0.1475 \log[HCO_3{}^-] - 0.2069\,pH$

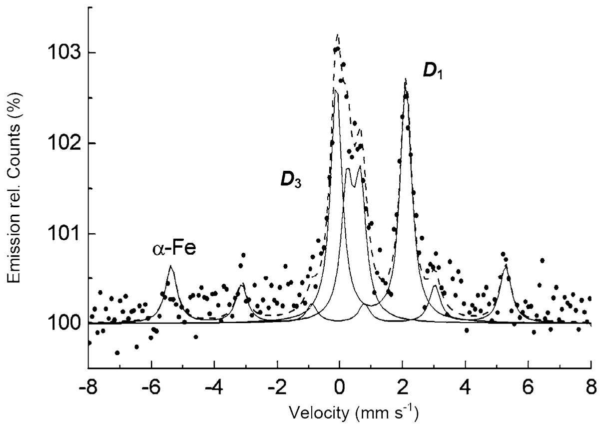

Fig. 2. CEMS spectrum at room temperature of a steel disk dipped during 24 h in a 0.1 M $NaHCO_3$ solution. ·······: Experimental curve, - - - - -: global computed curve, ——: components of the spectra.

Fig. 2. Spectre Mössbauer en électron de conversion (CEMS) à l'ambiante d'un disque d'acier trempé 24 h dans une solution de $NaHCO_3$ à 0,1 mol l^{-1}. ········ : courbe expérimentale, - - - - - : courbe globale calculée, —— : composantes du spectre.

It stabilised then at -450 mV_{SHE} as the corrosion of iron proceeded. The green rust layer obtained after 24 h was analysed by CEMS at room temperature in the inert atmosphere of the gas flow proportional counter. The spectrum (Fig. 2) is composed of three spectral components, two doublets due to a paramagnetic compound and one sextet due to a magnetically ordered compound. The hyperfine parameters of this sextet prove to be typical of α-Fe at room temperature. This is the signal coming from the substrate, detected because the rust layer is porous and does not cover completely the metal. The hyperfine parameters of the doublets D_1 ($\delta = 1.10$ mm s^{-1} and $\Delta = 2.22$ mm s^{-1}) and D_3 ($\delta = 0.55$ mm s^{-1} and $\Delta = 0.42$ mm s^{-1}) are characteristic of Fe^{II} and Fe^{III} atoms in a GR compound [38]. Since only carbonate species were present in the solution, this GR can only be the hydroxycarbonate of chemical formula $Fe^{II}{}_4Fe^{III}{}_2(OH)_{12}CO_3{\cdot}3H_2O$. The D_1/D_3 area ratio, which is practically identical to the Fe^{II}/Fe^{III} ratio within the GR, is measured at 1.8 ($\equiv 35.7\%$ Fe^{III}), very close indeed to the awaited value of 2 ($\equiv 33.3\%$ Fe^{III}). Moreover, a slight discrepancy due to the small emission percent comes from ignoring a second ferrous doublet D_2, the intensity of which should be (1/3) that of D_1. Consequently, the value that is computed must lie between 1.5 and 2. The measured value of the OCP is thus reported in the Pourbaix diagram (Fig. 1). The pH of the 0.1 M $NaHCO_3$ solution is buffered at about 8.3 by the hydrogenocarbonate ions and the corresponding point is represented by a ringed cross, which is located at the centre of the domain of stability of $GR(CO_3{}^{2-})$.

When NaCl is added to the 0.1 M $NaHCO_3$ solution, the green rust layer resulting of the immersion at OCP of iron disks is still composed of the hydroxycarbonate, even for NaCl concentration of 4 M [1]. This illustrates the well-known stability of the hydroxycarbonate structure with respect to any other form of GRs and in particular those obtained with monovalent anions [26,27,37]. But the results are different if the corrosion process is accelerated electrochemically. Galvanostatic experiments were performed on iron electrodes dipped in a 0.6 M $NaHCO_3 + 0.5$ M NaCl solution of pH about 8.3 [16]. The corrosion product was a mixture of 35% $GR(CO_3{}^{2-})$ with 65% $FeCO_3$. In this case, siderite $FeCO_3$ forms, whereas it is not obtained at the OCP. Similarly, the dissolution of E24 steel electrodes anodically polarised in a 0.1 M $NaHCO_3 + 0.02$ M NaCl solution mainly leads to $FeCO_3$ [42]. The difference between the behaviour at OCP and the behaviour under anodic polarisation is likely a consequence of the influence of $\{[Fe^{2+}{}_{aq}]/[OH^-]\}$ and $\{[HCO_3{}^- + CO_3{}^{2-}]/[OH^-]\}$ concentration ratios. If they are small, $Fe(OH)_2$ can

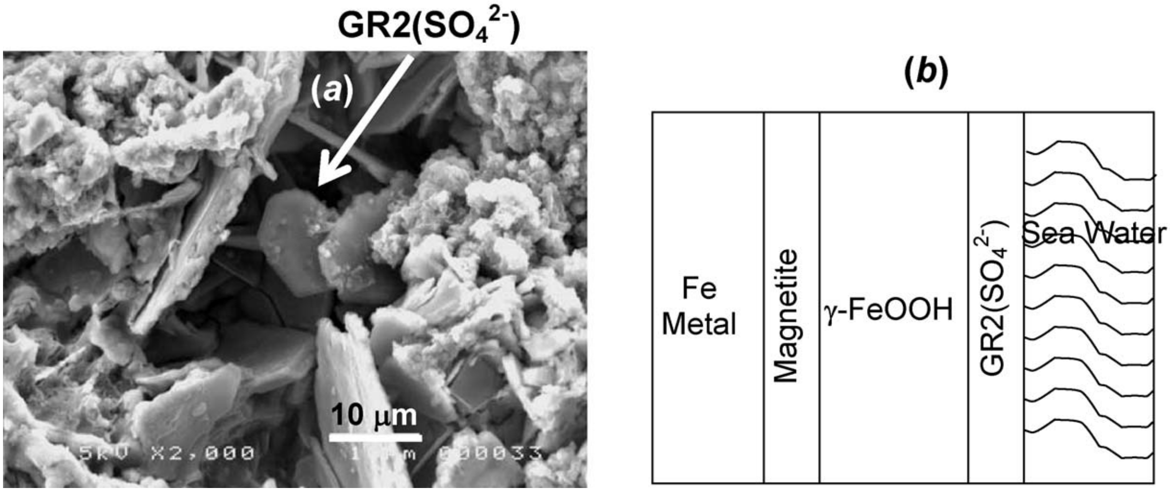

Fig. 3. (**a**) SEM micrograph showing hexagonal shaped crystals of GR(SO_4^{2-}) upon corroded steel sheet left 25 years in seawater and (**b**) sequence of the rust layers: metal–magnetite–lepidocrocite–GR(SO_4^{2-}) [40].

Fig. 3. (**a**) Micrographie par microscopie électronique à balayage montrant des cristaux hexagonaux de rouille verte carbonatée sur une feuille d'acier corrodé abandonnée 25 ans dans l'eau de mer et (**b**) séquence des couches de rouille : métal–magnétite–lépidocrocite–rouille verte sulfatée [40].

precipitate and is rapidly and totally transformed into GR(CO_3^{2-}). An increase of these ratios should favour $FeCO_3$ at the expense of $Fe(OH)_2$. At the OCP, the reduction of O_2 produces two OH^- ions when the dissolution of iron produces one Fe^{2+}. This should favour GR(CO_3^{2-}). When an anodic polarisation is applied, the reduction of O_2 does not match the production of Fe^{2+} ions, thus favouring $FeCO_3$.

5. Seawater, GR(SO_4^{2-}) and microbially influenced corrosion

Ten- to fifteen-millimetre-thick rust layers formed on steel sheet piles during 25 years proved to be composed of three main layers [40]. The inner one, close to the metal substrate, is essentially made of magnetite. The intermediate one is composed of iron(III) oxyhydroxides. Finally, in the external one, the closest to the interface with seawater, the sulphated form of GRs proved to be the main constituent (Fig. 3). A Raman spectrum of this GR(SO_4^{2-}) is displayed (Fig. 4). In agreement with the previous Raman studies of GRs [6,7,21,45], it is composed of two intense peaks at 430 and 508 cm^{-1}, that were attributed to Fe^{II}–OH and Fe^{III}–OH stretching, respectively [6,7]. The weaker band at 260 cm^{-1} was more rarely mentioned [21]. Chemical analyses demonstrated that the GR contained elements Fe, O and S, indicating that it was the hydroxysulphate [40]. However, the Cl^-/SO_4^{2-} molar ratio in seawater is about 19. This illustrates once more the affinity of the GR structure for divalent anions. Note that in seawater the main carbonate species is HCO_3^- but SO_4^{2-} is overwhelming, since $\{[SO_4^{2-}]/[HCO_3^-]\}$ molar ratio is about 12. This explains why GR(SO_4^{2-}) forms even though CO_3^{2-} produces a better stability of the layered structure of GRs [26,27,37].

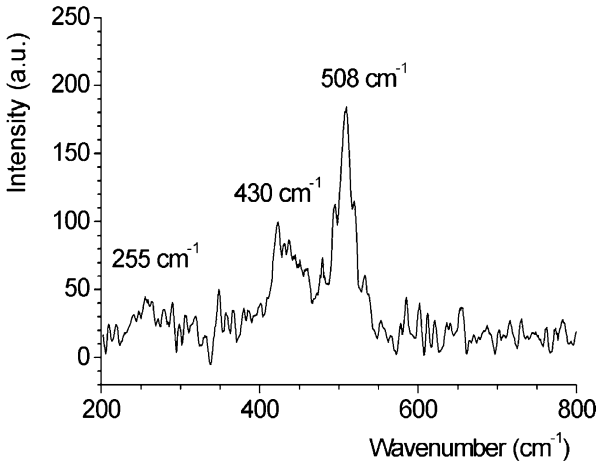

Fig. 4. Raman spectrum of the outer part of a marine corrosion rust layer formed on steel.

Fig. 4. Spectre Raman de la partie externe d'une couche de rouille formée par corrosion marine sur l'acier.

Additional experiments were performed in the laboratory in order to study the competition between GR(Cl^-) and GR(SO_4^{2-}). The oxidation of a precipitate obtained by mixing solutions of $FeCl_2{\cdot}4\,H_2O$,

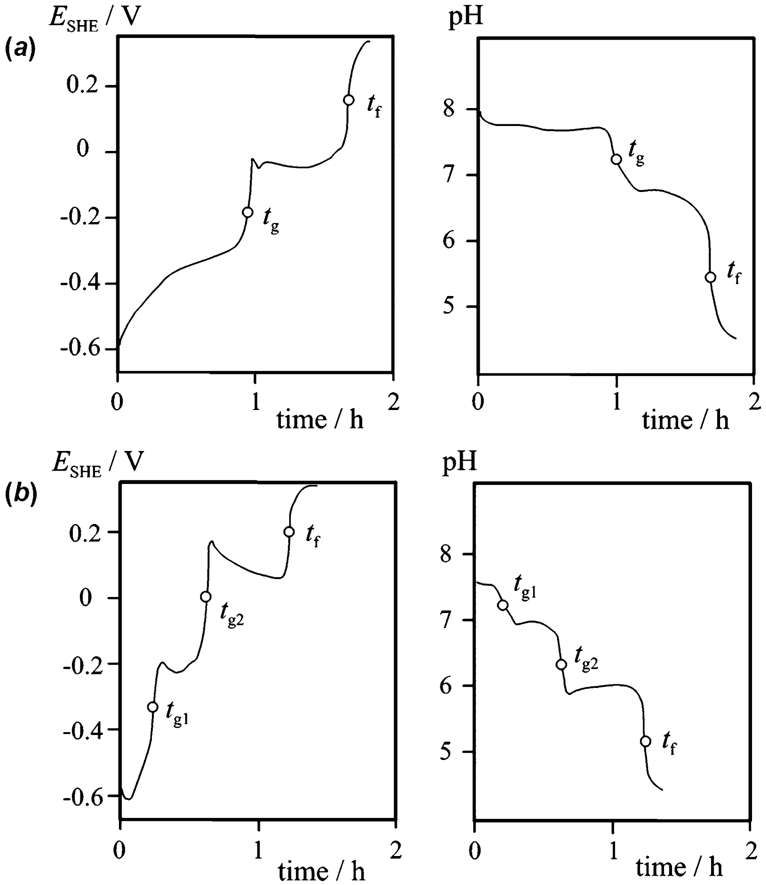

Fig. 5. E_{SHE} (V vs. SHE) and pH vs. time curves obtained during the oxidation of aqueous suspensions of Fe(II)-containing precipitates in the presence of Cl^- and SO_4^{2-} ions. $[Cl^-]/[SO_4^{2-}] = 12$. (**a**) $[Fe^{2+}]/[OH^-] = 0.58$; (**b**) $[Fe^{2+}]/[OH^-] = 1$.

Fig. 5. Courbes E_{SHE} (V par rapport à l'électrode standard à hydrogène, SHE) et pH en fonction du temps, obtenues au cours de l'oxydation de suspensions aqueuses de précipités contenant du Fe^{II} en présence d'ions Cl^- et SO_4^{2-}. $\{[Cl^-]/[SO_4^{2-}]\} = 12$. (**a**) $\{[Fe^{2+}]/[OH^-]\} = 0.58$; (**b**) $\{[Fe^{2+}]/[OH^-]\} = 1$.

$FeSO_4{\cdot}7\,H_2O$ and NaOH was studied. The Cl^-/SO_4^{2-} molar ratio was set at 12, whereas two $\{[Fe^{2+}]/[OH^-]\}$ ratios, 0.58 and 1, were considered. The redox potential E and pH versus time curves are displayed in Fig. 5. Those obtained for $\{[Fe^{2+}]/[OH^-]\} = 0.58$ are typical of a two-stage reaction involving the formation of a GR compound as an intermediate product. The first stage elapses from $t = 0$ to t_g and corresponds to the formation of a GR from the initial Fe^{II} compound, the second one elapses from t_g to t_f and corresponds to the oxidation of the GR into FeOOH phases releasing Fe^{II} and anions into solution. Large E and pH variations of around t_g and t_f testify of the disappearance of an initial phase [38,39]. In contrast, the curves obtained for $\{[Fe^{2+}]/[OH^-]\} = 1$ indicate that the reaction involves a supplementary stage, a first one ending at t_{g1}, a second one at t_{g2} and the third one at t_f.

Intermediate compounds were analysed by XRD. Patterns are displayed in Fig. 6. The GR found at t_g for $\{[Fe^{2+}]/[OH^-]\} = 0.58$ is identified as $GR(SO_4^{2-})$ (Fig. 6a). The three main diffraction lines at $2\theta = 9.25°$ (1.1 nm), 18.69° (0.55 nm) and 28.22° (0.367 nm) are characteristic of a hydroxysulphate XRD pattern and correspond to (001), (002) and (003) lines of the trigonal structure [46]. Some lines of lepidocrocite γ-FeOOH, end-product of the oxidation process and faint lines of $GR(SO_4^{2-})$ of other indices than (00ℓ) are also detected. The abnormal intensity of the (00ℓ) lines is due to preferential orientation of $GR(SO_4^{2-})$ microcrystallites. Thus, in this case, where $\{[Cl^-]/[SO_4^{2-}]\} = 12$ and $\{[Fe^{2+}]/[OH^-]\} = 0.58$, $GR(SO_4^{2-})$ forms instead of $GR(Cl^-)$ even though SO_4^{2-} is in minority, a consequence of the affinity of GRs for divalent anions. The XRD pattern of the product obtained at t_{g2} for $\{[Fe^{2+}]/[OH^-]\} = 1$ is almost identical to the pre-

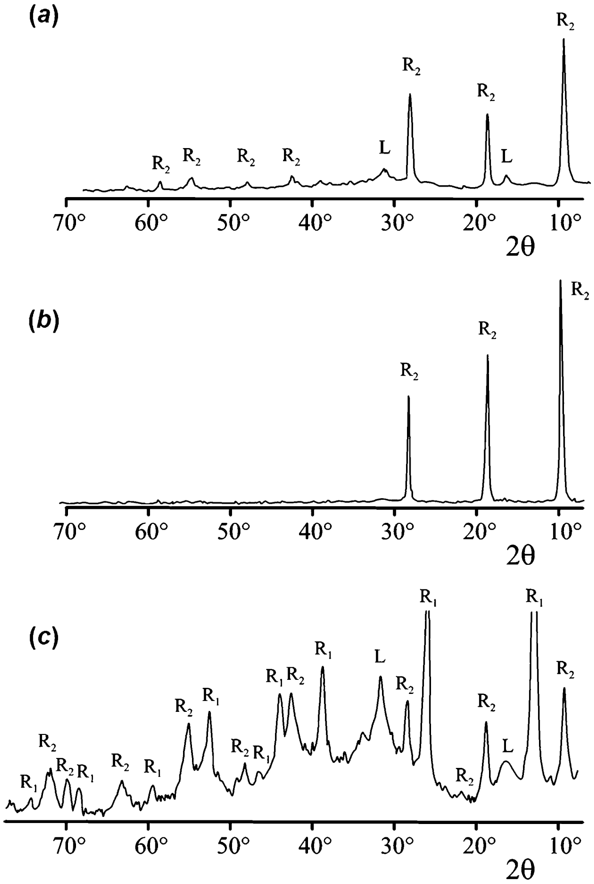

Fig. 6. XRD patterns of the intermediate products obtained by oxidation of aqueous suspensions of Fe(II)-containing precipitates in the presence of Cl^- and SO_4^{2-} ions. $[Cl^-]/[SO_4^{2-}] = 12$. $\lambda(Co\,K\alpha_1) = 0.17889$ nm. (**a**) Product obtained at t_g for $[Fe^{2+}]/[OH^-] = 0.58$; (**b**) product obtained at t_{g2} for $[Fe^{2+}]/[OH^-] = 1$; (**c**) product obtained at t_{g1} for $[Fe^{2+}]/[OH^-] = 1$. R_1 are the lines of GR(Cl^-), R_2 are the lines of GR(SO_4^{2-}), and L are diffraction lines of lepidocrocite.

Fig. 6. Clichés de diffraction des rayons X des produits intermédiaires obtenus par oxydation de suspensions aqueuses de précipités contenant du Fe(II) en présence d'ions Cl^- et SO_4^{2-}. $[Cl^-]/[SO_4^{2-}] = 12$. $\lambda(Co\,K\alpha_1) = 0.17889$ nm. (**a**) Produit obtenu à t_g pour $[Fe^{2+}]/[OH^-] = 0,58$; (**b**) produit obtenu à t_{g2} pour $[Fe^{2+}]/[OH^-] = 1$; (**c**) produit obtenu à t_{g1} pour $[Fe^{2+}]/[OH^-] = 1$. R_1 désigne les raies de GR(Cl^-), R_2 celles de GR(SO_4^{2-}), et L celles de la lépidocrocite.

vious one (Fig. 6b). GR(SO_4^{2-}) is also obtained here. However, the XRD pattern of the product obtained at t_{g1} is mainly composed of the diffraction lines of GR(Cl^-) (Fig. 6c). They are denoted R_1. Two of them, at $2\theta = 12.92°$ (0.795 nm) and 25.98° (0.398 nm), are extremely intense and correspond to (003) and (006) lines of the conventional hexagonal cell of the rhombohedral structure [38]. Therefore, the first reaction stage corresponds to the formation of GR(Cl^-) from the initial precipitate, the second stage to the oxidation of GR(Cl^-) into GR(SO_4^{2-}) and the last stage to the oxidation of GR(SO_4^{2-}) into γ-FeOOH. The diffraction lines of GR(SO_4^{2-}), denoted R_2, are seen, together with those of GR(Cl^-), as a result of the oxidation of GR(Cl^-). Similarly, the two main diffraction lines of γ-FeOOH, denoted L, can be noticed.

GR(SO_4^{2-}) proved to have a well defined composition of $Fe^{II}_4Fe^{III}_2(OH)_{12}SO_4{\cdot}8\,H_2O$ [15,39,46]. The average oxidation number of iron is then +2.33. In contrast, it was observed that the composition of GR(Cl^-) varied continuously [38] as the oxidation advanced. Starting from a compound with formula $Fe^{II}_3Fe^{III}(OH)_8Cl{\cdot}n\,H_2O$, chloride and Fe^{III} contents increased, up to an approximate composition of $Fe^{II}_{2.2}Fe^{III}(OH)_{6.4}Cl{\cdot}n'\,H_2O$. The average oxidation number of iron varied then from +2.25 to +2.31. We may propose that in the presence of SO_4^{2-} anions, the enrichment in Cl^- and Fe^{III} is replaced by a transformation of $Fe^{II}_3Fe^{III}(OH)_8Cl{\cdot}n\,H_2O$ into GR(SO_4^{2-}) and obviously sulphate anions deliver a phase that is more stable than that obtained with chloride anions. The differences observed between the oxidation processes at $\{[Fe^{2+}]/[OH^-]\} = 1$ and 0.58 may result from the nature of the initial precipitate. When $\{[Fe^{2+}]/[OH^-]\}$ is small, close to 0.5, the value corresponding to the stoichiometric conditions of formation of $Fe(OH)_2$, the initial precipitate is indeed $Fe(OH)_2$ or close to $Fe(OH)_2$ [35]. When $\{[Fe^{2+}]/[OH^-]\}$ is larger, Fe(II)-hydroxychlorides may form [35]. At $\{[FeCl_2]/[NaOH]\} = 2.5$, the initial precipitate was identified as β-$Fe_2(OH)_3Cl$ [36]. This compound gets oxidised the way $Fe(OH)_2$ does into $Fe^{II}_3Fe^{III}(OH)_8Cl{\cdot}n\,H_2O$, and we may suppose that, even in the presence of sulphate ions, the oxidation of such an hydroxychloride leads to GR(Cl^-). The oxidation of β-$Fe_2(OH)_3Cl$ into $Fe^{II}_3Fe^{III}(OH)_8Cl{\cdot}n\,H_2O$ could well be a solid-state reaction.

We demonstrated previously that in marine environments the dissolution of iron in seawater should lead to GR(SO_4^{2-}). Some severe cases of corrosion are due to the concomitant presence of sulphate-reducing bacteria (SRB) and of GR(SO_4^{2}) among the corrosion products [14,30]. The recent paper that described carefully the sequence of rust stratification on steel sheet piles at the anoxic level of sea mud suggests that it is due to bacterial reduction of previously formed lepidocrocite where large hexagonal GR(SO_4^{2-}) crystals are clearly identified (Fig. 3) [40]. We thus propose that GR(SO_4^{2-}) forms firstly due to the reduction of γ-FeOOH in the outer layer by ubiquitous dissimilatory iron-reducing bacteria (DIRB). Then, the zone enriched in $GR(SO_4^{2-})$ is favourable to the colonisation of the interface by other micro-organisms, the sulphate-reducing bacteria (SRB). SRBs then induce formation of H_2S, which is an acidification of the environment, which results in a drastic increase of iron degradation. Microbially influenced corrosion of steels would then be a two-step process involving DIRB that form $GR(SO_4^{2-})$ followed by the reduction of this sulphate reservoir by SRBs.

6. Oxidation of GRs and formation of rust

Other phases can also be obtained from GRs in more specific conditions. Akaganeite forms from $GR(Cl^-)$ in solutions containing a large excess of $Fe^{2+}{}_{aq}$ and Cl^- [36]. Ferrihydrite was also reported to form from $GR(Cl^-)$, when the Fe concentration is very low and the oxidation kinetics fast [41]. Phosphate species modify considerably the oxidation process of aqueous suspensions of $GR(CO_3^{2-})$. For instance, in a first article, the final product was unambiguously identified as ferrihydrite [3], but more recently it was concluded that this product was a 'ferric green rust', that is a Fe^{III} compound characterised by a layered structure similar to that of GRs [23]. The existence of such 'ferric green rusts' demonstrates clearly that Fe^{II} cations can be oxidised in situ and that the structure of GRs can sustain up to 100% Fe^{III} [17,34,41]. In order to compensate for the increase in positive charge, the oxidation of Fe^{II} is accompanied by a deprotonation of the OH^- ions of the brucite-like layers. Ferric GRs can be obtained by oxidation of GRs with hydrogen peroxide [4,34,41], electrochemical polarisation of iron [21] or aerial oxidation of dried GR layers [1]. The formation of the ferric $GR(CO_3^{2-})$ was reinvestigated here in the case of steel corrosion.

First, a $GR(CO_3^{2-})$ layer was grown on a steel electrode left at OCP in a 0.1 M $NaHCO_3$ solution, as described here in part 3. The sample was removed from the solution and left in the dry atmosphere of the laboratory. The deep-green corrosion layer turned progressively to brown and was analysed one month later by XRD. Secondly, a 10-ml solution containing approximately 30% H_2O_2 was added to an aqueous suspension of $GR(CO_3^{2-})$ prepared with the procedure described previously [3]. The suspension turned immediately to brown and the precipitate was filtered, dried to powder and analysed by XRD. Both XRD patterns are presented in Fig. 7.

The two most intense lines visible in the pattern of the dried rust layer are those of the substrate α-Fe. Lines

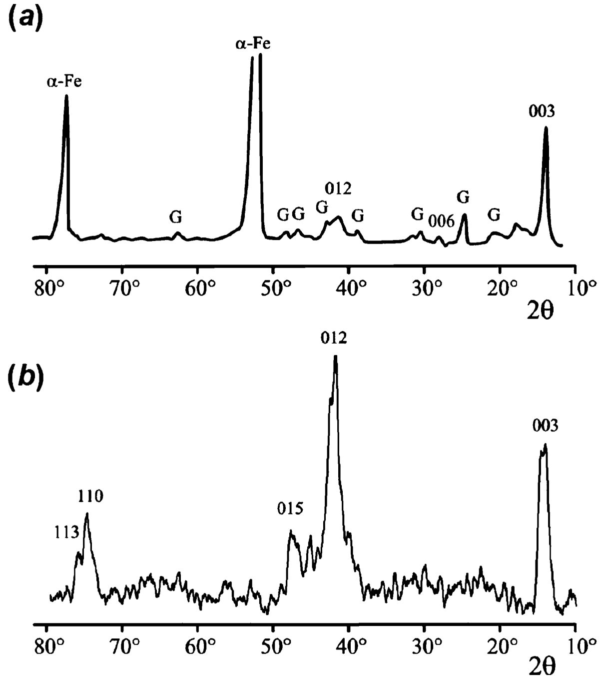

Fig. 7. XRD patterns of the 'ferric $GR(CO_3^{2-})$'. The lines denoted by their Miller indices *hkl* can be ascribed to the 'ferric green rust' (see text). $\lambda(\mathrm{Co\,K}\alpha_1) = 0.17889$ nm. (**a**) Rust layer obtained by aerial oxidation of a $GR(CO_3^{2-})$ layer formed on steel after 5 days of immersion in a 0.1 M $NaHCO_3$ solution. G are the diffraction lines of goethite and α-Fe those of the substrate. (**b**) Compound obtained by addition of H_2O_2 to an aqueous suspension of $GR(CO_3^{2-})$.

Fig. 7. Clichés de diffraction de rayons X de la « rouille verte $GR(CO_3^{2-})$ ferrique ». Les raies désignées par les indices *hkl* peuvent être attribuées à la rouille verte ferrique (voir le texte). $\lambda(\mathrm{Co\text{-}K}\alpha_1) = 0.17889$ nm. (**a**) Couche de rouille obtenue par oxydation à l'air d'une couche de rouille verte carbonatée, formée après 5 jours sur un acier dans une immersion en une solution de $NaHCO_3$ à 0,1 $\mathrm{mol\,l^{-1}}$. G désigne les raies de la goethite et α-Fe celles du substrat. (**b**) Composé obtenu par adition de H_2O_2 à une suspension aqueuse de rouille verte carbonatée.

of goethite α-FeOOH are also observed, together with three other lines that can be attributed to the ferric GR. The main one corresponds to an interplanar distance of 0.735 nm ($2\theta = 14°$), that is the distance d_{003} between interlayers. The occurrence of this peak in the pattern of the 'ferric GR' definitively proves that the sequence among hydroxide and anionic layers is conserved in the structure. The decrease of d_{003} from 0.750 nm in $GR(CO_3^{2-})$ [13] to 0.735 nm in 'ferric GR' is attributed to the decrease of the ionic diameter of iron species, from 0.156 nm for Fe^{II} to 0.129 nm for Fe^{III} [44]. Two other peaks are visible, at 0.3675 nm ($2\theta = 28.2°$) and 0.254 nm ($2\theta = 41.3°$).

The pattern obtained by oxidation of $GR(CO_3^{2-})$ with hydrogen peroxide is composed of five main lines that can all be attributed also to 'ferric $GR(CO_3{}^{2-})$'. Assuming that the ferric GR keeps the pyroaurite structure of $GR(CO_3{}^{2-})$ [2], it is computed that the observed diffraction lines are indeed associated with intense lines of the GR structure. The parameters of the conventional hexagonal cell are determined at $a = 0.301$ nm and $c = 2.205$ nm. The corresponding Miller index (*hkl*) was then used to identify the 'ferric GR' diffraction lines on the patterns of Fig. 6. However, it is not possible to exclude that ferrihydrite forms together with the ferric GRs if the conditions of corrosion are inhomogeneous as it is surely in actual cases. As a matter of fact, the most poorly ordered form of ferrihydrite, the so-called two-line ferrihydrite, is characterised by an XRD pattern made of two broad lines at $2\theta \sim 42°$ and $74°$. Intense lines of the ferric GR are also located in these angular regions and may mask those of ferrihydrite.

7. Conclusion

The determining role of GRs in the corrosion processes of ferrous alloys in neutral and alkaline media is now well settled. $Fe^{II–III}$ hydroxysalts constitute a major step before the formation of the various components of rust and may control partially the properties of the rust layers formed on steel. Therefore, the positive role of various corrosion inhibitors commonly used to prevent degradation of steels in neutral or alkaline media are partially explained by the influence those species may have upon the formation and/or transformation of GRs. Phosphates, nitrites and nitrates are examples of such inhibitors.

References

[1] M. Abdelmoula, P. Refait, S.H. Drissi, J.-P. Mihé, J.-M.R. Génin, Conversion electron Mössbauer spectroscopy and X-ray diffraction studies of the formation of carbonate-containing green rust one by corrosion of metallic iron in $NaHCO_3$ and ($NaHCO_3$ + NaCl) solutions, Corros. Sci. 38 (1996) 623–633.

[2] R. Allmann, The crystal structure of pyroaurite, Acta Crystallogr. B 24 (1968) 972–977.

[3] O. Benali, M. Abdelmoula, P. Refait, J.-M.R. Génin, Effect of orthophosphate on the oxidation products of Fe(II)–Fe(III) hydroxycarbonate: the transformation of green rust to ferrihydrite, Geochim. Cosmochim. Acta 65 (2001) 1715–1726.

[4] J.D. Bernal, D. Dasgupta, A.L. Mackay, The oxides and hydroxides of iron and their structural inter-relationships, Clay Miner. Bull. 4 (1959) 15–30.

[5] B. Beverskog, I. Puigdomenech, Revised Pourbaix diagrams for iron at 25–300 °C, Corros. Sci. 38 (1996) 2121–2135.

[6] N. Boucherit, A. Hugot-Le Goff, S. Joiret, Raman studies of corrosion films grown on Fe and Fe–6 Mo in pitting conditions, Corros. Sci. 32 (1991) 497–507.

[7] N. Boucherit, A. Hugot-Le Goff, S. Joiret, In situ Raman identification of stainless steels pitting corrosion films, Mater. Sci. Forum 111–112 (1992) 581–588.

[8] J. Bruno, P. Wersin, W. Stumm, On the influence of carbonate in mineral dissolution: II. The solubility of $FeCO_{3(s)}$ at 25 °C and 1 atm total pressure, Geochim. Cosmochim. Acta 56 (1992) 1149–1155.

[9] G. Butler, J.G. Beynon, The corrosion of mild steel in boiling salt solutions, Corros. Sci. 7 (1967) 385–404.

[10] R. Derie, M. Ghodsi, Contribution à l'étude de la formation des sesquioxydes de Fe(III) monohydrates par aération de gels d'hydroxyde de Fe(II), Ind. Chim. Belg. 37 (1972) 731–740.

[11] J. Detournay, L. De Miranda, R. Derie, M. Ghodsi, The region of stability of green rust II in the electrochemical potential–pH equilibrium diagram of iron in sulphate medium, Corros. Sci. 15 (1975) 295–306.

[12] J. Detournay, R. Derie, M. Ghodsi, Etude de l'oxydation par aération de $Fe(OH)_2$ en milieu chlorure, Z. Anorg. Allg. Chem. 427 (1976) 265–273.

[13] S.H. Drissi, P. Refait, M. Abdelmoula, J.-M.R. Génin, Preparation and thermodynamic properties of Fe(II)–Fe(III) hydroxycarbonate (green rust 1), Pourbaix diagram of iron in carbonate-containing aqueous media, Corros. Sci. 37 (1995) 2025–2041.

[14] J.-M.R. Génin, A.A. Olowe, N.D. Benbouzid-Rollet, D. Prieur, M. Confente, B. Resiak, The simultaneous presence of green rust 2 and sulphate reducing bacteria in the corrosion steel sheet piles in a harbour area, Hyperfine Interact. 69 (1991) 875–878.

[15] J.-M.R. Génin, A.A. Olowe, P. Refait, L. Simon, On the stoichiometry and Pourbaix diagram of Fe(II)–Fe(III) hydroxysulphate or sulphate-containing green rust 2: an electrochemical and Mössbauer spectroscopy study, Corros. Sci. 38 (1996) 1751–1762.

[16] J.-M.R. Génin, L. Dhouibi, P. Refait, M. Abdelmoula, E. Triki, Influence of phosphate on corrosion products of iron in chloride-polluted-concrete-simulating solutions: ferrihydrite vs. green rust, Corrosion 58 (2002) 467–478.

[17] J.-M.R. Génin, A. Rabha, A. Géhin, M. Abdelmoula, O. Benali, V. Ernstsen, G. Ona-Nguema, C. Upadhyay, C. Ruby, Fougerite and $Fe^{II–III}$ hydroxycarbonate green rust; ordering, deprotonation and/or cation substitution; structure of hydrotalcite-like compounds and mythic ferrosic hydroxide $Fe(OH)_{(2+x)}$, Solid-State Sci. 7 (2005) 545–572.

[18] H.C.B. Hansen, Composition, stabilisation, and light absorption of Fe(II)–Fe(III) hydroxycarbonate (green rust), Clay Miner. 24 (1989) 663–669.

[19] D.L. Jensen, J.K. Boddum, J.C. Tjell, T.H. Christensen, The solubility of rhodochrosite ($MnCO_3$) and siderite ($FeCO_3$) in anaerobic aquatic environments, Appl. Geochim. 17 (2002) 503–511.

[20] G.H. Kelsall, R.A. Williams, Electrochemical behaviour of ferrosilicides (Fe_xSi) in neutral and alkaline aqueous electrolytes, J. Electrochem. Soc. 138 (1991) 931–940.

[21] L. Legrand, G. Sagon, S. Lecomte, A. Chaussé, R. Messina, A Raman and infrared study of a new carbonate green rust obtained by electrochemical way, Corros. Sci. 43 (2001) 1739–1749.

[22] L. Legrand, R. Maksoub, G. Sagon, S. Lecomte, J.-P. Dallas, A. Chaussé, Electroanalytical and kinetic investigations on the carbonate green rust-Fe(III) redox system, J. Electrochem. Soc. 150 (2003) B45–B51.

[23] L. Legrand, L. Mazerolles, A. Chaussé, The oxidation of carbonate green rust into ferric phases: solid state reaction or transformation via solution, Geochim. Cosmochim. Acta 68 (2004) 3497–3507.

[24] I.R. McGill, B. McEnaney, D.C. Smith, Crystal structure of green rust formed by corrosion of cast iron, Nature 29 (1976) 200–201.

[25] J.-B. Memet, P. Girault, R. Sabot, C. Compère, C. Deslouis, Electrochemical impedance spectroscopy of a free-standing oxide film, Electrochim. Acta 47 (2002) 1043–1053.

[26] A. Mendiboure, R. Schöllhorn, Formation and anion exchange reactions of layered transition metal hydroxides $[Ni_{1-x}M_x](OH)_2(CO_3)_{x/2}$ $(H_2O)_z$ ($M =$ Fe,Co), Rev. Chim. Miner. 23 (1986) 819–827.

[27] S. Miyata, Anion exchange properties of hydrotalcite-like compounds, Clays Clay Miner. 31 (1983) 305–311.

[28] A.A. Olowe, J.-M.R. Génin, The mechanism of oxidation of ferrous hydroxide in sulphated aqueous media: importance of the initial ratio of the reactants, Corros. Sci. 32 (1991) 965–984.

[29] A.A. Olowe, J.-M.R. Génin, The influence of concentration on the oxidation of ferrous hydroxide in acidic sulphated aqueous medium: Particle size analysis of lepidocrocite, Corros. Sci. 32 (1991) 1021–1028.

[30] A.A. Olowe, A. Bauer, J.-M.R. Génin, J. Guézennec, Mössbauer effect evidence of the existence of green rust 2 transient compound from bacterial corrosion in marine sediments, Corrosion NACE 45 (1989) 229–234.

[31] A.A. Olowe, J.-M.R. Génin, J. Guézennec, Mössbauer effect study of microbially induced corrosion of steel by sulfate reducing bacteria in marine sediments: Role of green rust 2, in: T.N. Knoxville, N.J. Dowling, M.W. Mitleman, J.C. Danko (Eds.), Microbially Influenced Corrosion and Deterioration, The University of Tennessee and NACE, 1990, pp. 65–72.

[32] A.A. Olowe, B. Pauron, J.-M.R. Génin, The influence of temperature on the oxidation of ferrous hydroxide in sulphated aqueous medium: activation energies of formation of the products and hyperfine structure of magnetite, Corros. Sci. 32 (1991) 985–1001.

[33] P. Refait, J.-M.R. Génin, The oxidation of Fe(II) hydroxide in chloride-containing aqueous media and Pourbaix diagrams of green rust 1, Corros. Sci. 34 (1993) 797–819.

[34] P. Refait, J.-M.R. Génin, The oxidation of Ni(II)–Fe(II) hydroxides in chloride-containing aqueous media, Corros. Sci. 34 (1993) 2059–2070.

[35] P. Refait, J.-M.R. Génin, Chloride-containing ferrous hydroxides, in: "ICAME95", in: SIF Conference Proceedings, vol. 50, SIF, Bologna, Italy, 1996, pp. 55–58.

[36] P. Refait, J.-M.R. Génin, The mechanisms of oxidation of ferrous hydroxychloride β-$Fe_2(OH)_3Cl$ in aqueous solution: the formation of akaganeite vs. goethite, Corros. Sci. 39 (1997) 539–553.

[37] P. Refait, S.H. Drissi, J. Pytkiewicz, J.-M.R. Génin, The anionic species competition in iron aqueous corrosion: role of various green rust compounds, Corros. Sci. 39 (1997) 1699–1710.

[38] P. Refait, M. Abdelmoula, J.-M.R. Génin, Mechanism of formation and structure of green rust one in aqueous corrosion or iron in the presence of chloride ions, Corros. Sci. 40 (1998) 1547–1560.

[39] P. Refait, C. Bon, L. Simon, G. Bourrié, F. Trolard, J. Bessière, J.-M.R. Génin, Chemical composition and Gibbs free energy of formation of Fe(II)–Fe(III) hydroxysulphate green rust and Fe(II) hydroxide, Clay Miner. 34 (1999) 499–510.

[40] P. Refait, J.-B. Memet, C. Bon, R. Sabot, J.-M.R. Génin, Formation of the Fe(II)–Fe(III) hydroxysulphate green rust during marine corrosion of steel, Corros. Sci. 45 (2003) 833–845.

[41] P. Refait, O. Benali, M. Abdelmoula, J.-M.R. Génin, Formation of 'ferric green rust' and/or ferrihydrite by fast oxidation of iron(II–III) hydroxychloride green rust, Corros. Sci. 45 (2003) 2435–2449.

[42] M. Reffass, R. Sabot, C. Savall, M. Jeannin, J. Creus, P. Refait, Localised corrosion of carbon steel in $NaHCO_3$/NaCl electrolytes: role of Fe(II)-containing compounds, Corros. Sci. 48 (2006) 709–726.

[43] J.J. Santana Rodriguez, F.J. Santana Hernandez, J.E. Gonzalez Gonzalez, XRD and SEM studies of the layer of corrosion products for carbon steel in various different environments in the province of Las Palmas (The Canary Islands, Spain), Corros. Sci. 44 (2002) 2425–2438.

[44] R.D. Shannon, Revised effective ionic radii and systematic studies of interatomic distances in halides and chalcogenides, Acta Crystallogr. A 32 (1976) 751–767.

[45] S. Simard, M. Odziemkowski, D.E. Irish, L. Brossard, H. Ménard, In situ micro-Raman spectroscopy to investigate pitting corrosion product of 1024 mild steel in phosphate and bicarbonate solutions containing chloride and sulphate ions, J. Appl. Electrochem. 31 (2001) 913–920.

[46] L. Simon, M. François, P. Refait, G. Renaudin, M. Lelaurain, J.-M.R. Génin, Structure of Fe(II–III) layered double hydroxysulphate green rust two from Rietveld analysis, Solid-State Sci. 5 (2003) 327–334.

[47] P.P. Stampfl, Ein basisches Eisen-II–III-Karbonat in Rost, Corros. Sci. 9 (1969) 185–187.

[48] D.D. Wagman, W.H. Evans, V.B. Parker, R.H. Schumm, I. Halow, S.M. Bailey, K.L. Churney, R.L. Nutall, The NBS tables of chemical thermodynamic properties. Selected values for inorganic and C1 and C2 organic substances in SI units, J. Phys. Chem. Ref. Data 11 (suppl. 2) (1982).